© 2026. Published by The Company of Biologists | Journal of Cell Science (2026) 139, jcs264687. doi:10.1242/jcs.264687

SHORT REPORT

Lgl antagonizes Par complex membrane association to enable neural stem cell asymmetric division

Sarah E. Welch*, Bryce LaFoya* and Kenneth E. Prehoda‡

ABSTRACT

The Par complex regulates cell polarity in diverse animal cells, but how it is restricted to a specific membrane domain remains unclear. The tumor suppressor Lethal giant larvae (Lgl) is thought to inhibit Par complex membrane binding, yet in metaphase *Drosophila* neural stem cells (NSCs), Lgl is cytoplasmic while the Par complex is apically polarized, raising the question of how Lgl controls Par localization when it is not on the membrane. Using live imaging, we found that Lgl and atypical Protein Kinase C (aPKC) exhibit tightly coordinated, opposing membrane dynamics: aPKC displaces Lgl at mitotic entry, while Lgl displaces aPKC at mitotic exit. In Lgl-depleted NSCs, aPKC is not fully cleared from the membrane after mitosis, and this residual aPKC persists into the subsequent division, disrupting Miranda polarization. Apical aPKC recruitment still occurs, indicating that Lgl is not required for Par polarization per se, but rather for ensuring aPKC absence from the basal membrane before mitosis. These findings reveal a temporal mode of mutual antagonism between Lgl and the Par complex that may license proper asymmetric division.

KEY WORDS: Polarity, Tumor suppressor, Asymmetric cell division

INTRODUCTION

Cortical polarity is a fundamental cellular characteristic that underlies diverse biological processes, including directional cell migration, tissue organization, and asymmetric cell division. The Par complex, consisting of Par-6 and atypical Protein Kinase C (aPKC), plays a pivotal role in establishing and maintaining polarity in a wide range of animal cells, from epithelial cells to neurons (Lang and Munro, 2017; Venkei and Yamashita, 2018; Sunchu and Cabernard, 2020; Buckley and St Johnston, 2022). The proper localization and function of the Par complex are particularly important in stem cells, where asymmetric distribution of cell fate determinants governs the delicate balance between self-renewal and differentiation. A fundamental question in cell polarity research is how the Par complex itself is restricted to a specific membrane domain. The tumor suppressor Lethal giant larvae (Lgl) plays a key role in inhibiting Par association with the membrane (Bell et al., 2015; Carvalho et al., 2015; Grifoni et al., 2007; Yamanaka et al., 2006; Moreira and Morais-de-Sá, 2016), but how Lgl controls Par complex localization remains an open question.

Institute of Molecular Biology, Department of Chemistry and Biochemistry, 1229 University of Oregon, Eugene, OR 97403, USA.
*These authors contributed equally to this work

‡Author for correspondence (prehoda@uoregon.edu)

K.E.P., 0000-0003-4214-6158

Handling Editor: Richa Rikhy
Received 24 December 2025; Accepted 27 March 2026

Par polarity is the result of a complex interplay of positive and negative regulators. While factors such as Par-3 (Bazooka in *Drosophila*) and Cdc42 ensure that the Par complex is targeted to the membrane (Holly et al., 2020; Atwood et al., 2007; Hutterer et al., 2004), the negative regulation provided by Lgl [l(2)gl in *Drosophila*; hereafter Lgl] restricts the complex to a specific membrane domain. Lgl is thought to perform this crucial function by spatial exclusion, whereby Lgl prevents the Par complex from binding to membrane regions where it is localized (Buckley and St Johnston, 2022; Bell et al., 2015; Carvalho et al., 2015; Lee et al., 2006b). The spatial exclusion model is exemplified by interphase epithelial cells, where the Par complex is confined to the apical plasma membrane while Lgl occupies the basolateral domain (Fig. 1A). In the absence of Lgl function, the Par complex enters the basolateral domain (Bailey and Prehoda, 2015; Dong et al., 2015; Betschinger et al., 2003; Bell et al., 2015; Carvalho et al., 2015; Yamanaka et al., 2006).

Like epithelial cells, proper Par function in neural stem cells (NSCs) requires Lgl (Rolls et al., 2003; Peng et al., 2000; Ohshiro et al., 2000; Bell et al., 2015). However, a key difference between the behavior of Lgl in NSCs and epithelia lies in the localization of Lgl. Instead of localizing to the basal membrane where the Par complex is excluded, Lgl is cytoplasmic whereas the Par complex is polarized in NSCs (Bell et al., 2015) (Fig. 1A). Polarized Par complex with cytoplasmic Lgl has also been observed in sensory organ precursor (SOP) cells (Wirtz-Peitz et al., 2008), further challenging the spatial exclusion model.

RESULTS AND DISCUSSION

Patterned Lgl membrane dynamics during NSC mitosis

To gain insight into how Lgl regulates Par complex localization in NSCs, we first examined the membrane localization dynamics of Lgl, including how it is restored to the membrane following mitosis. We imaged the localization of Lgl in NSCs from *Drosophila* larval brain explants expressing Lgl-GFP (expressed from its endogenous locus) (Fig. 1B,C). Lgl removal from the membrane (i.e. reduction below our limit of detection, which does not exclude the possibility of low-level membrane association) began in early prophase, initiating at a small area near the apical pole of the cell and continuing rapidly across the membrane appearing to be completely removed by late prophase (Fig. 1C,D; Movie 1). We also imaged Lgl-GFP expressed using UAS-GAL4, and found that the localization of Lgl expressed in this manner was indistinguishable from the expression from the endogenous locus, but the signal was improved (Fig. 1C′,D′; Movie 1).

Whereas Lgl appeared to be completely removed from the membrane of NSCs in intact tissue, the Lgl signal from progeny cells adhered to the basal region prevented a definite determination. We imaged individual cultured NSCs that had been dissociated from brains to observe basal Lgl dynamics in the absence of adhering cells. The Lgl dynamics in dissociated NSCs were consistent with our initial observations of apically directed membrane clearing and confirmed that Lgl is indeed completely removed from the

Journal of Cell Science (2026) 139, jcs264687. doi:10.1242/jcs.264687

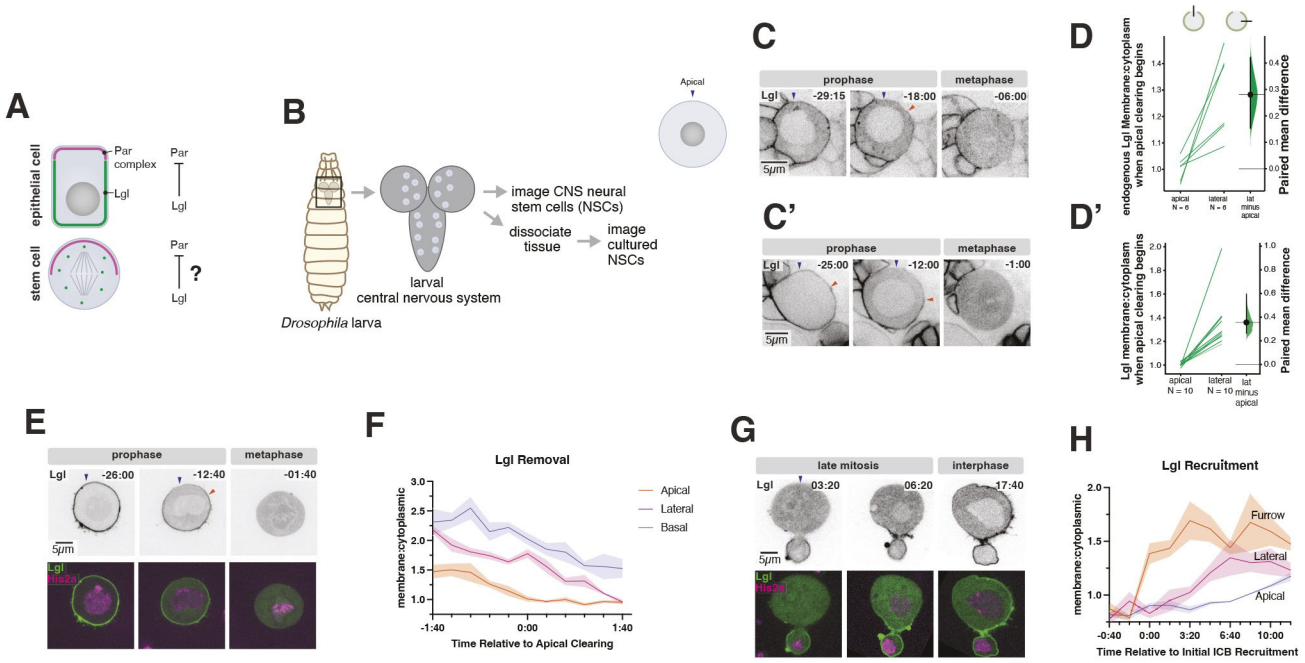


Fig. 1. Patterned Lgl displacement and reloading during neural stem cell asymmetric division. (A) Lgl regulation of Par complex localization in epithelial and neural stem cells. In epithelial cells, the tumor suppressor Lethal Giant Larvae (Lgl; green) localizes to the basolateral membrane, restricting the Par complex (magenta) to the apical membrane. Lgl also restricts the Par complex to the apical membrane of metaphase *Drosophila* neural stem cells (NSCs); however, Lgl itself is cytoplasmic at metaphase. How does Lgl inhibit basal Par complex localization when it is not on the NSC membrane? (B) Imaging *Drosophila* larval brain NSCs. The larval central nervous system (CNS), including the brain lobes and ventral nerve cord, was extracted from third-instar larvae (L3). NSCs were characterized by their large size, specific locations within the brain, and expression of tissue-specific transgenes. NSCs were either imaged within the intact CNS or in isolation after dissociation of the CNS tissue. (C) Lgl localization dynamics during NSC asymmetric division. Lgl expressed from its endogenous promoter was imaged in NSCs from the intact CNS. Selected frames from Movie 1 are shown with blue arrowheads indicating the apical side of the NSC and the orange arrowhead indicating the boundary of Lgl removal from the apical membrane. Time (min:s) is shown relative to anaphase onset. (C′) Lgl localization dynamics during NSC asymmetric division. UAS-Lgl-GFP driven by the NSC-specific driver Worniu-Gal4. Blue arrowheads indicate the apical side of the NSC, while the orange arrowheads indicate the boundary of Lgl removal from the apical membrane. Time (min:s) is shown relative to anaphase onset. Frames from Movie 1 are shown. (D) Quantification of Lgl removal from the plasma membrane from the intact CNS expressed under its endogenous promoter. The ratio of membrane-to-cytoplasmic Lgl was measured from the apical and lateral regions of each cell, as shown in the schematic above (n=6). Measurements were taken at the initial frame when the apical membrane-to-cytoplasmic ratio reached 1, indicating initial removal of Lgl. The Gardner–Altman estimation plot illustrates the paired measurements from each NSC. Additionally, the 95% confidence interval is displayed in the mean difference comparison, along with the corresponding bootstrap distribution from which it was derived. (D′) Quantification of Lgl removal from the plasma membrane in NSCs from the intact CNS expressing UAS-Lgl-GFP driven by Worniu-Gal4. Measurements were taken using the method described above for D. The Gardner–Altman estimation plot illustrates the paired measurements from each NSC (n=10). Additionally, the 95% confidence interval is displayed in the mean difference comparison, along with the corresponding bootstrap distribution from which it was derived. (E) Lgl localization dynamics during dissociated NSC division. NSC with Lgl-GFP driven by Worniu-Gal4/UAS and Histone H2A (His2a-RFP). Blue arrowheads indicate the apical side of the NSC, while the orange arrowhead indicates the boundary of Lgl removal from the apical membrane. Time (min:s) is shown relative to anaphase onset. Frames from Movie 1 are shown. (F) Time course of Lgl removal from the plasma membrane from dissociated NSCs. The membrane-to-cytoplasmic ratio was measured from the apical, lateral and basal regions of each NSC (n=3). Time point zero indicates initial Lgl removal, defined as the frame in which the Lgl membrane-to-cytoplasmic ratio first reaches 1. Measurements were taken beginning 1 min and 40 s before initial Lgl removal, during initial Lgl removal, and for 1 min and 40 s following initial Lgl removal. Shaded areas represent 1 s.d. (G) Lgl recruitment dynamics dissociated NSC division. NSC is expressing UAS-Lgl-GFP driven by Worniu-Gal4 and Histone H2A (His2a-RFP). The blue arrowhead indicates the apical side of the NSC. Time (min:s) is shown relative to initial recruitment to the intercellular bridge (ICB). (H) Time course of Lgl recruitment to the plasma membrane during mitotic exit from dissociated NSCs. The membrane-to-cytoplasmic ratio was measured using the same method described for F. Time point zero indicates initial Lgl recruitment to the NSC plasma membrane, defined as the time point at which the membrane-to-cytoplasmic ratio exceeded 1 at the intracellular bridge (ICB). Measurements were taken beginning 40 s before initial recruitment, and continued for 11 min and 40 s after initial recruitment. Shaded areas represent 1 s.d.

membrane by late prophase (Fig. 1E,F; Movie 1). The patterned Lgl membrane displacement dynamics indicate that removal is a spatially regulated process, like that observed for SOP cells (Wirtz-Peitz et al., 2008), rather than one in which Lgl is simultaneously removed from all over the membrane.

NSCs undergo repeated cycles of asymmetric division, requiring that Lgl be restored to the membrane to re-establish its interphase localization. We observed that Lgl reloading began during late cytokinesis on the plasma membrane near the intercellular bridge (Fig. 1G,H; Movies 1, 3). Reloading rapidly continued until Lgl was fully around the plasma membrane in early interphase. The overall pattern of Lgl reloading in NSCs is similar to that observed in follicular epithelial cells (Moreira et al., 2019). Our results provide a detailed description of the dynamic localization of Lgl throughout the cell cycle in NSCs, revealing precise spatial and temporal control of its membrane association.

Lgl is removed from the NSC plasma membrane by aPKC

Since Lgl is cytoplasmic when the Par complex is polarized in metaphase NSCs, we sought to understand how Lgl transitions between membrane-bound and cytoplasmic states. Evidence from various cell types indicates that Lgl can be phosphorylated and

Journal of Cell Science (2026) 139, jcs264687. doi:10.1242/jcs.264687

removed from the membrane by the Par complex subunit aPKC but also by the mitotic kinase Aurora A (Bell et al., 2015; Carvalho et al., 2015). Aurora A could also regulate the membrane association of Lgl indirectly by influencing aPKC polarity (Wirtz-Peitz et al., 2008; Lee et al., 2006a). We sought to determine whether one or both kinases are responsible for the patterned removal of Lgl from the NSC membrane during prophase. To dissect the relative contributions of aPKC and Aurora A to Lgl removal, we separately inhibited aPKC or Aurora A activity and assessed the effect on Lgl localization dynamics. We inhibited aPKC by expressing a UAS-controlled aPKC-RNAi specifically in larval brain NSCs using Worniu-GAL4 driven expression. For Aurora A inhibition, we added the specific inhibitor MLN8237 (Carvalho et al., 2015) to the larval brain explant culture media. We note that the RNAi inhibition is chronic while the inhibitor inhibition is acute.

In NSCs in which aPKC was depleted by RNAi, we observed that Lgl removal from the membrane in mitosis was largely inhibited (Fig. 2A,B; Movie 2). Unlike wild-type NSCs, in which Lgl was removed from the membrane late in prophase, aPKC-RNAi NSCs had persistent Lgl membrane enrichment throughout mitosis. We did detect a small decrease in apical Lgl membrane signal beginning in early prophase (Fig. 2A,B; Movie 2), suggesting the presence of residual aPKC activity or a small contribution from another mechanism. The retention of Lgl on the membrane in aPKC-depleted cells indicates that aPKC-mediated phosphorylation is the primary mechanism driving Lgl dissociation from the plasma membrane as NSCs enter mitosis.

We also tested whether Aurora A activity is required for Lgl membrane displacement as it can directly phosphorylate Lgl and can also regulate aPKC polarity (Bell et al., 2015; Carvalho et al., 2015; Wirtz-Peitz et al., 2008; Lee et al., 2006a). We did not detect an effect on Lgl localization in MLN8237-treated NSCs (Fig. 2C,D; Movie 2). The patterned removal of Lgl from the membrane proceeded with similar dynamics and extent as observed in untreated cells. However, we did observe cytokinesis defects in MLN8237-treated NSCs (Fig. 2C′; Movie 2) indicating that Aurora A was successfully inhibited. We conclude that, despite its known ability to phosphorylate Lgl, Aurora A does not participate in the removal of Lgl from the NSC membrane. This conclusion is consistent with a previous study demonstrating that Aurora A phosphorylation sites on Lgl are not required for NSC membrane displacement (Bell et al., 2015).

Coupling and uncoupling of aPKC and Lgl membrane dynamics during NSC division

We next sought to determine the degree to which aPKC and Lgl membrane dynamics are spatially and temporally correlated. The recruitment of aPKC to the membrane in early prophase is a complex, multistep process whereby aPKC is initially localized to small domains on the apical membrane before coalescing into an apical cap by metaphase (Oon and Prehoda, 2019, 2021). To determine the interplay between the disappearance of Lgl and the appearance of aPKC on the membrane, we simultaneously imaged aPKC-GFP (expressed from its endogenous promoter) and Lgl-mCherry (expressed by Worniu-GAL4 driven UAS) in NSCs. This approach allowed us to directly

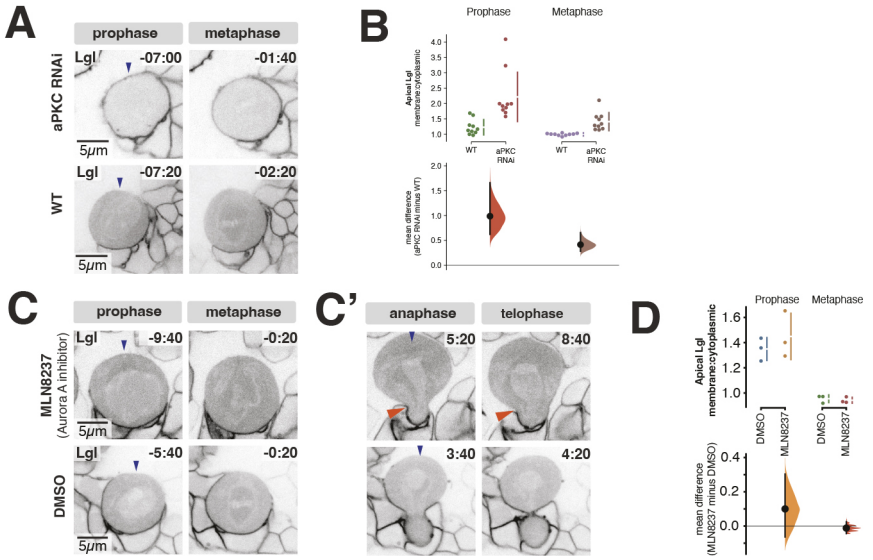


Fig. 2. aPKC but not Aurora A is required for Lgl removal from the NSC membrane in early mitosis. (A) Lgl dynamics in NSCs within the intact CNS expressing aPKC RNAi. Frames from Movie 2 are shown. The NSC is expressing UAS-Lgl-GFP and UAS-aPKC-RNAi, both driven by the *Drosophila* NSC-specific driver Worniu-Gal4. Time (min:s) is shown relative to anaphase onset. The same time points are shown for an NSC expressing UAS-Lgl-GFP, but not UAS-aPKC-RNAi, for a wild-type (WT) comparison. Blue arrowheads indicate the apical side of the cell. (B) aPKC is required for Lgl removal from the membrane in early mitosis. The membrane-to-cytoplasmic ratio of Lgl signal on the apical side of the cell was measured for NSCs expressing aPKC-RNAi and for cells expressing UAS-Lgl-GFP but not aPKC-RNAi for the WT condition. Cells were measured at both prophase and metaphase. The Gardner–Altman estimation plot displays error bars, indicating one s.d. (with the gap representing the mean). The bar in the mean difference comparison reflects the bootstrap 95% confidence interval. Each data point corresponds to a measurement taken from a distinct NSC (n=10). (C) Lgl dynamics in an NSC from the intact CNS incubated with the specific Aurora A inhibitor MLN8237. Frames from Movie 2 are shown. Time (min:s) is shown relative to anaphase onset. Blue arrowheads indicate the apical side of the cell. For comparison, similar time points are depicted for an NSC incubated with DMSO alone (vehicle control). (C′) Cytokinetic defects in NSCs incubated with the Aurora A inhibitor MLN8237. Frames from Movie 2 are shown. Time (min:s) is shown relative to anaphase onset. Blue arrowheads indicate the apical side of the cell, while the orange arrowheads indicate furrow retraction during late cytokinesis, providing evidence of drug effectiveness. For comparison, similar time points are depicted for an NSC incubated in DMSO alone (vehicle control). (D) Aurora A inhibition does not detectably influence Lgl membrane displacement in early mitosis. Lgl apical membrane-to-cytoplasmic ratio is shown for NSCs incubated with either MLN237 or the vehicle control (DMSO) during prophase and metaphase. The Gardner–Altman estimation plot displays error bars representing one s.d. (with gap indicating the mean). The bar representing the mean difference comparison reflects the bootstrap 95% confidence interval.

Journal of Cell Science (2026) 139, jcs264687. doi:10.1242/jcs.264687

observe the spatial and temporal dynamics of aPKC recruitment with the pattern of Lgl removal from the cell membrane. Lgl removal at the apical pole of the NSC was tightly correlated with the appearance of aPKC at that site (Fig. 3A-C; Movie 3). In the apical hemisphere, the appearance of aPKC at the membrane was strongly correlated with Lgl removal. However, Lgl was also removed from the basal membrane even though aPKC does not localize there. We conclude that aPKC removes Lgl from the membrane both directly (i.e. apical membrane) and indirectly (i.e. basal membrane). Indirect removal of basal Lgl by apical aPKC is likely influenced by factors such as the rate of Lgl diffusion along the plasma membrane.

Near the end of mitosis, aPKC spreads along the nascent NSC membrane while being excluded from the membrane of the smaller nascent neural precursor (Oon and Prehoda, 2019) (Fig. 3C; Movie 3). Shortly after it reached the furrow, aPKC was removed from the membrane. We observed patterned removal of aPKC from the membrane that was correlated with the membrane reloading of Lgl at mitotic exit (Figs 1G,H, 3C,D; Movie 3). As Lgl accumulated on the basal membrane of the nascent NSC near the intercellular bridge, aPKC was removed from the membrane in a complementary pattern. Lgl continued to spread along the membrane until it occupied both basal and apical membrane and aPKC was no longer detectable on the membrane (Fig. 3C-E).

Lgl is required for aPKC removal from the membrane at mitotic exit

The spatial exclusion model, which posits that Lgl excludes aPKC from membrane regions where Lgl is bound, does not explain the role of Lgl in regulating aPKC localization in SOP cells (Wirtz-Peitz et al., 2008) or NSCs (Bell et al., 2015) (Fig. 3A). In each cell type, while Lgl activity is required for proper aPKC localization, aPKC is polarized to one membrane hemisphere whereas Lgl is cytoplasmic. This raises the question of how Lgl regulates the association of aPKC with the mitotic NSC basal membrane when Lgl itself is cytoplasmic. Our data demonstrate that Lgl is reloaded on the NSC membrane in late cytokinesis simultaneously with the displacement of aPKC into the cytoplasm. This tight temporal correlation led us to examine whether Lgl is required for aPKC removal from the membrane at mitotic exit. To test this hypothesis, we examined aPKC localization in NSCs expressing Lgl-RNAi (Worniu-GAL4-driven UAS). Whereas aPKC is excluded from the cell membrane during interphase in wild-type NSCs, aPKC was not removed from the membrane at the end of mitosis in Lgl-RNAi NSCs, remaining on the membrane throughout interphase and the subsequent mitosis (Fig. 4A-C; Movie 4). This persistence indicates that Lgl is required for complete aPKC clearance from the NSC membrane at mitotic exit. In wild-type NSCs, aPKC accumulates at the apical membrane during early mitosis and we observed a similar accumulation in NSCs expressing Lgl-RNAi (Fig. 4A,D; Movie 4). Thus, aPKC is polarized in both wild-type and Lgl-RNAi NSCs, with the key difference being that the basal membrane of wild-type NSCs lacks aPKC whereas the basal membrane of Lgl-RNAi NSCs contains the residual aPKC that was not cleared at the end of the previous mitosis. These observations indicate that the aPKC present on the basal membrane during mitosis in Lgl-depleted NSCs originates from the failure of clearance at the preceding mitotic exit.

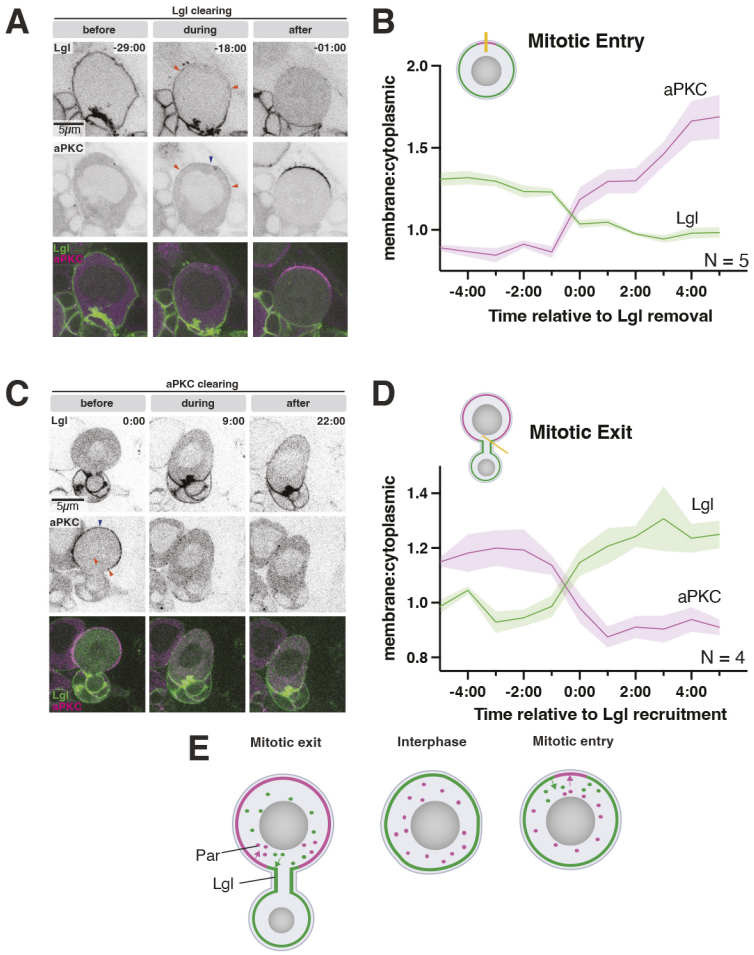


Fig. 3. aPKC displaces Lgl at mitotic entry and Lgl displaces aPKC at mitotic exit. (A) Lgl and aPKC dynamics in an NSC from the intact CNS during Lgl membrane clearance at mitotic entry. Frames from Movie 3 are shown. The NSC is expressing aPKC-GFP (expressed from its native promoter) and UAS-Lgl-mCherry driven by Worniu-Gal4. Time (min:s) is indicated relative to anaphase onset. The blue arrowhead indicates the apical side of the cell, while the orange arrowheads indicate the boundary of aPKC membrane signal. (B) Time course of Lgl removal and aPKC recruitment at mitotic entry. The apical membrane-to-cytoplasmic ratio of Lgl and aPKC was assessed throughout mitotic entry for intact CNS NSCs (n=6). Time point zero indicates the frame in which Lgl is initially removed from the apical membrane (defined as the frame in which Lgl membrane-to-cytoplasmic ratio first reaches 1; see schematic). Measurements were taken beginning 5 min prior to initial Lgl removal, and ending 5 min after initial Lgl removal. Shaded areas represent 1 s.d. (C) Lgl and aPKC dynamics in an NSC from the intact CNS during Lgl membrane recruitment and aPKC membrane clearance during mitotic exit. Frames from Movie 3 are shown. The NSC is expressing aPKC-GFP (expressed from its native promoter) and UAS-Lgl-mCherry, driven by Worniu-Gal4. Time (min:s) is indicated relative to anaphase onset. The blue arrowhead indicates the apical side of the cell, while the orange arrowheads indicate the boundary of aPKC signal. (D) Lgl recruitment and aPKC removal at mitotic exit. The membrane-to-cytoplasmic ratio at the intracellular bridge (ICB; see schematic) was measured as indicated above (n=7). Time point zero indicates the frame in which Lgl is initially recruited to the ICB (defined as the first frame in which the ICB Lgl signal exceeds 1). Measurements were taken beginning 5 min before initial Lgl recruitment and ending 5 min after. (E) Schematic of Lgl and aPKC dynamics in NSCs. In wild-type cells, Lgl (green) is initially recruited near the ICB, while aPKC (magenta) is simultaneously removed from near the ICB at mitotic exit to establish the interphase state, in which Lgl is fully membrane-bound and aPKC is cytoplasmic. Beginning at mitotic entry, recruitment of aPKC to the apical membrane spatially and temporally coincides with Lgl membrane removal.

Journal of Cell Science (2026) 139, jcs264687. doi:10.1242/jcs.264687

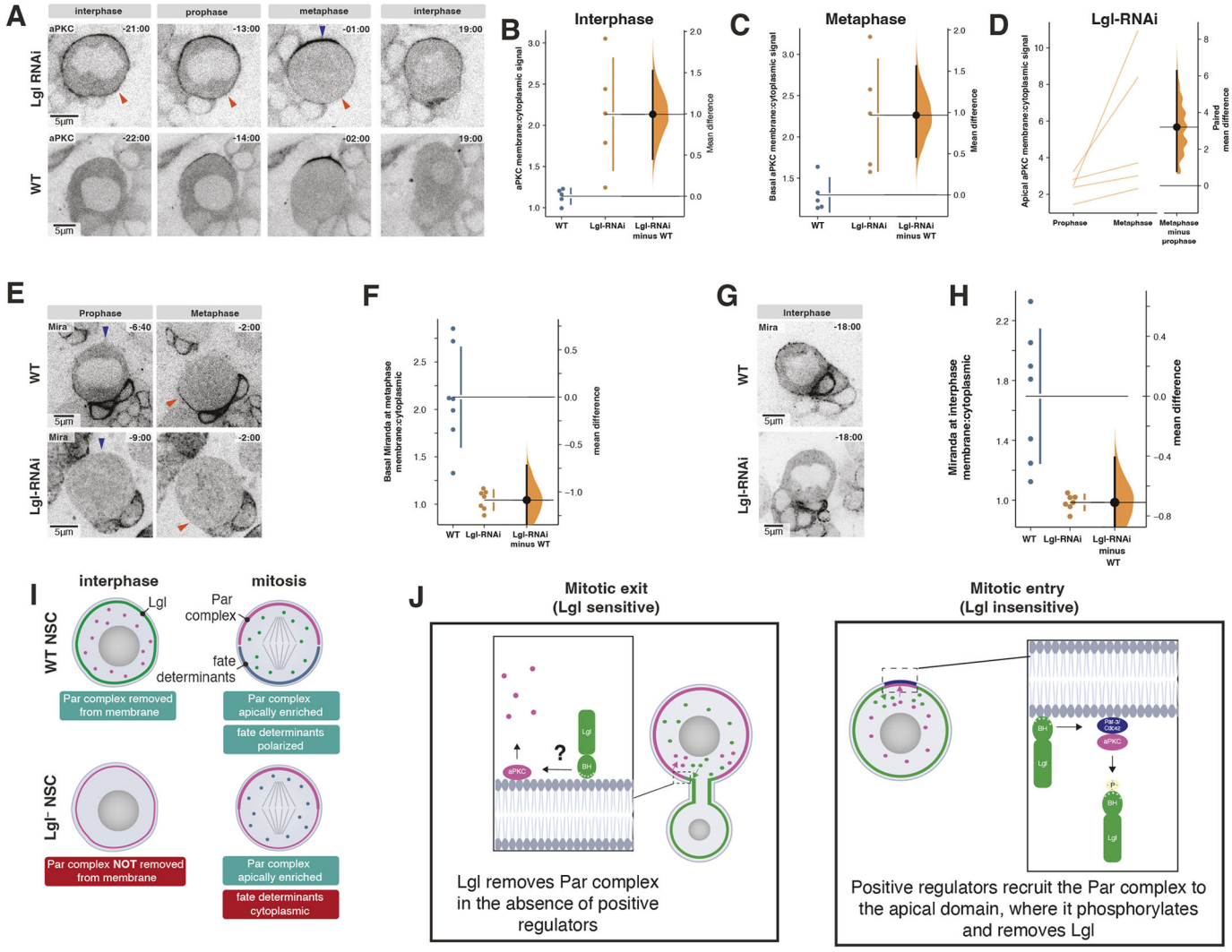


Fig. 4. See next page for legend.

Lgl is required for Miranda polarity

Given the failure of NSCs to fully clear aPKC from the membrane at the end of mitosis upon loss of Lgl, we next examined how this perturbation impacted fate determinant localization. Miranda is an adapter protein that traffics the fate determinants Prospero, Staufen and Brat into only the differentiating daughter cell, where they act to promote differentiation (Ikeshima-Kataoka et al., 1997; Shen et al., 1997; Schuldt et al., 1998; Matsuzaki et al., 1998; Lee et al., 2006c; Betschinger et al., 2006). The membrane association of Miranda is tightly regulated by aPKC, which phosphorylates its positively charged BH domain, thereby neutralizing the charge and preventing interaction with the negatively charged phosphate head groups of the plasma membrane (Bailey and Prehoda, 2015). In wild-type NSCs, this mechanism restricts Miranda to the basal crescent during mitosis. However, in Lgl-RNAi NSCs, Miranda failed to form a basal crescent at metaphase, consistent with the presence of ectopic basal aPKC (Fig. 4E,F; Movie 4). Moreover, whereas wild-type Miranda displays punctate membrane association during interphase, we observed little to no membrane association of Miranda in Lgl-depleted NSCs, suggesting that aPKC is active during interphase in these cells (Fig. 4G,H; Movie 4). Together, these observations indicate that Miranda is prevented from associating with the basal membrane of NSCs that lack Lgl function because of residual aPKC that was not cleared from the membrane. These results demonstrate that proper basal fate determinant localization requires the absence of aPKC from the basal membrane prior to mitotic polarization.

Lgl and the Par complex antagonize each other at distinct phases of the cell cycle

Lgl and the Par complex have been thought to regulate one another by ‘mutual exclusion’. In this mechanism, the presence of each component on the membrane leads to exclusion of the other. For example, Par complex on the apical membrane prevents Lgl from occupying the apical membrane (Peng et al., 2000; Yamanaka et al., 2006; Hutterer et al., 2004). How the Par complex excludes Lgl from the membrane is well understood. Lgl is a Par complex substrate and Lgl phosphorylation by the Par complex displaces it from the membrane (Hutterer et al., 2004; Graybill et al., 2007). No direct exclusion mechanism has been described for Lgl, however, and our results provide a more nuanced view of how Lgl regulates Par complex localization in NSCs than that provided by the mutual exclusion model. We observed that Lgl and the Par complex can control the localization of one another but at different time periods. Starting at early mitosis, the Par complex completely removes Lgl

Fig. 4. Lgl ensures aPKC is not on the membrane at the start of the NSC polarity cycle. (A) aPKC dynamics in an NSC from the intact CNS expressing Lgl-RNAi. Frames from Movie 4 are shown. The NSC is expressing aPKC-GFP driven by its native promoter, and UAS-Lgl-RNAi driven by Worniu-Gal4. The blue arrowhead indicates the apical side of the cell. The orange arrowheads indicate the presence of basal aPKC before and during mitosis. Time (min:s) is shown relative to anaphase onset. For comparison, an NSC that does not express Lgl-RNAi (wild type, WT) is shown at corresponding time points. (B) Lgl is required to remove aPKC from the membrane during the transition to interphase, but not for aPKC polarity. A comparison of apical aPKC membrane:cytoplasmic signal in NSCs both expressing and not expressing UAS-Lgl-RNAi during interphase. A Gardner–Altman estimation plot illustrates the data for five distinct NSCs. Error bars indicate one s.d., with the gap representing the mean. The bar in the mean difference comparison reflects the bootstrap 95% confidence interval. (C) In NSCs that lack Lgl, aPKC bound on the membrane during interphase leads to basal aPKC at metaphase. A comparison of basal aPKC membrane signal in NSCs both expressing and not expressing UAS-Lgl-RNAi during metaphase. A Gardner–Altman estimation plot illustrates the data for five distinct NSCs. Error bars indicate one s.d., with the gap representing the mean. The bar in the mean difference comparison reflects the bootstrap 95% confidence interval. (D) Lgl is not required for apical Par complex localization. A comparison of apical aPKC membrane:cytoplasmic signal in NSCs lacking Lgl during prophase and metaphase is shown. The paired mean difference between prophase and metaphase is shown in the Gardner–Altman estimation plot. Both groups are plotted on the left axes as a slope graph: each paired set of observations is connected by a line. The paired mean difference is plotted on a floating axes on the right as a bootstrap sampling distribution. The mean difference is depicted as a dot; the 95% confidence interval is indicated by the ends of the vertical error bar. (E) Miranda dynamics in an NSC from the intact CNS expressing Lgl-RNAi. Frames from Movie 4 are shown. The NSC is expressing Miranda-GFP driven by its native promoter, and UAS-Lgl-RNAi driven by Worniu-Gal4. Blue arrowheads indicate the apical side of the cell, while orange arrowheads indicate the presence or absence of basal Miranda signal. Time (min:s) is shown relative to anaphase onset. For comparison, an NSC that does not express Lgl-RNAi (WT) is shown at similar time points. (F) Lgl is required for basal Miranda crescent localization during metaphase. A comparison of basal Miranda membrane:cytoplasmic signal in NSCs both expressing and not expressing UAS-Lgl-RNAi during metaphase. A Gardner–Altman estimation plot illustrates the data for seven distinct NSCs. Error bars indicate one s.d., with the gap representing the mean. The bar in the mean difference comparison reflects the bootstrap 95% confidence interval. (G) Interphase Miranda dynamics in an NSC from an intact CNS expressing Lgl-RNAi. Frames from Movie 4 are shown. The NSC is expressing Miranda-GFP driven by its native promoter and UAS-Lgl-RNAi driven by Worniu-Gal4. Time (min:s) is shown relative to nuclear envelope breakdown. For comparison, an NSC that does not express Lgl-RNAi (WT) is shown at a corresponding time point. (H) Lgl is required for Miranda membrane localization during interphase. A comparison of apical Miranda membrane:cytoplasmic signal in NSCs both expressing and not expressing UAS-Lgl-RNAi during interphase. A Gardner–Altman estimation plot illustrates the data for seven distinct NSCs. Error bars indicate one s.d., with the gap representing the mean. The bar in the mean difference comparison reflects the bootstrap 95% confidence interval. (I) Model of Lgl function in NSC asymmetric division. Lgl (green) removes aPKC (magenta) from the membrane beginning at mitotic exit. Without Lgl, aPKC remains on the membrane throughout interphase and into the next polarity cycle. Lgl is not required for apical recruitment of aPKC such that NSCs lacking Lgl remain polarized since aPKC is more concentrated on the apical membrane. However, the residual aPKC on the basal membrane of NSCs lacking Lgl leads to the displacement of fate determinants, thereby disrupting asymmetric cell division. In this model, Lgl is required to clear aPKC from the membrane so that it will not be present on the basal membrane when polarization begins. Whether this clearance function operates specifically at mitotic exit or reflects ongoing antagonism throughout the cell cycle remains to be determined (see Discussion). (J) Temporal polarization model. The localization of aPKC and Lgl in NSCs indicates that there are distinct time periods in which either aPKC or Lgl dominate membrane localization. In early mitosis, aPKC is dominant as it removes Lgl completely from the membrane but at the end of mitosis the reverse occurs and Lgl completely removes aPKC. This difference in sensitivity may arise from the presence or absence of positive regulators, Par-3 and Cdc42, whose apical recruitment of the Par complex during mitotic entry protects it from Lgl-mediated removal, whereas their absence at mitotic exit permits Lgl to displace the Par complex from the membrane.

from the membrane. How then, does Lgl regulate metaphase Par polarity? Our results suggest that it does so indirectly, by influencing the pre-polarized state. Wild-type NSCs enter mitosis without Par complex on the membrane such that it can be specifically localized to the apical membrane. NSCs that lack Lgl function enter mitosis with residual Par complex localized throughout the membrane. In this case, even though Par complex is subsequently specifically recruited to the apical membrane, residual Par complex on the basal membrane disrupts fate determinant polarity. Thus, in NSCs the Par complex and Lgl exhibit temporally segregated antagonism: during mitosis, the Par complex displaces Lgl from the membrane, while at mitotic exit Lgl displaces the Par complex. A key question arising from these observations is whether the essential contribution of Lgl to polarity occurs specifically during the interphase clearance phase, or whether Lgl continuously opposes aPKC throughout the cell cycle.

Two models are consistent with our data. In the first, which we term the interphase clearance model, the primary function of Lgl is to remove aPKC from the membrane during the transition from mitosis to interphase, effectively licensing the subsequent round of asymmetric division. In this model, the critical event is the clearance itself: if aPKC is not removed, it persists on the basal membrane and disrupts fate determinant localization when the next mitosis occurs. In the second model, continuous antagonism, Lgl opposes aPKC membrane association throughout the entire cell cycle, possibly because of elevated aPKC levels rather than a specific failure of interphase clearance, which disrupts Miranda localization. Because our Lgl-RNAi approach depletes Lgl constitutively, the present data cannot formally distinguish between these models.

Several observations lead us to favor the interphase clearance model. First, Lgl is present on the membrane at high levels during the clearance phase and is undetectable during mitosis. While we cannot exclude the possibility that Lgl functions at sub-detectable concentrations during mitosis, there is currently no positive evidence for Lgl membrane association at this stage, and proposing mitotic function requires invoking activity below the detection limit. Second, the exchange between Lgl loading and aPKC displacement at mitotic exit is sharp and temporally coordinated, more consistent with a discrete clearance event than with gradual, ongoing competition. Third, the earliest observable defect in Lgl-depleted NSCs is the failure of aPKC clearance at mitotic exit, placing the initial disruption at this specific cell cycle transition rather than during mitosis itself.

An important caveat to the interphase clearance model is raised by the observation that Lgl and aPKC appear to influence each other's localization even when one protein is at very low levels (Fig. 3). This raises the possibility that Lgl could function at the membrane during mitosis at concentrations below our detection limit. If so, Lgl might contribute to polarity through low-level membrane association throughout the cell cycle, consistent with continuous antagonism and obviating the need to invoke a specific interphase clearance event. Distinguishing between these possibilities will require temporally controlled perturbation approaches.

A related open question concerns the function of the aPKC that remains on the membrane when Lgl is depleted. Our data show that aPKC levels drop substantially but are not fully cleared in Lgl-RNAi NSCs (Fig. 4A-C), and that this residual aPKC is associated with Miranda displacement from the basal membrane. Whether this residual aPKC is enzymatically active, and whether there is a

threshold of basal aPKC below which Miranda can localize normally, remains to be determined. Combining Lgl depletion with partial reduction of aPKC levels could determine whether it is the absolute level of aPKC on the basal membrane during mitosis, rather than the specific failure of clearance, that accounts for the Miranda localization defect.

In temporal mutual exclusion, signaling events in the cell somehow control whether the Par complex or Lgl is dominant. In wild-type NSCs, Lgl removes the Par complex throughout interphase beginning at mitotic exit, whereas the Par complex dominates throughout mitosis. What might determine which factor is dominant in temporal mutual exclusion? Our data suggest that switching between Par complex and Lgl may depend on whether Par complex recruitment signals such as Cdc42 and Par-3 (Bazooka in *Drosophila*) are present. In this model, the Par complex is dominant when these signals are present, but Lgl becomes dominant when they are removed. In the absence of Lgl function, the Par complex is not completely displaced from the membrane in the absence of positive signals, perhaps because of an intrinsic, moderate affinity for the membrane that can be suppressed by Lgl. In this model, Lgl is not required for Par complex polarization per se, because the Par complex is recruited asymmetrically regardless of whether Lgl is present. Instead, the role of Lgl is to oppose Par complex membrane association during the phase when positive recruitment signals are absent, the functional consequence of which is to clear residual aPKC that would otherwise disrupt fate determinant localization.

The mechanism by which Lgl removes aPKC from the membrane at the end of mitosis remains an intriguing question. There are several possibilities based on our current understanding of Lgl and aPKC. One potential mechanism is that Lgl, upon its rapid return to the membrane post-mitosis, could act as a competitive inhibitor for aPKC membrane binding sites. The strong affinity of Lgl for the membrane (Bailey and Prehoda, 2015; Dong et al., 2015) might allow it to outcompete aPKC and displace it from the membrane. Alternatively, Lgl could recruit or activate a phosphatase that dephosphorylates aPKC or its binding partners. It is also possible that Lgl does not actively displace aPKC but rather regulates its steady-state membrane occupancy, such that loss of Lgl shifts the equilibrium toward higher aPKC levels at all cell cycle phases. In this scenario, the incomplete clearance observed in Lgl-depleted NSCs would reflect oscillation around an elevated baseline rather than failure of a specific displacement mechanism. Further investigation into these potential mechanisms will be crucial for fully understanding the role of Lgl in polarity regulation.

Limitations

The primary limitation of this study is that our Lgl-RNAi approach depletes Lgl constitutively throughout the cell cycle. As a result, we cannot determine whether Lgl is required specifically during the interphase clearance phase, during mitosis, or both. Distinguishing the interphase clearance model from continuous antagonism will require temporally controlled perturbation of Lgl function with resolution in the order of minutes within a single cell cycle. Additionally, our imaging approach defines Lgl 'removal' as reduction below the detection limit, and we cannot exclude the possibility that Lgl retains functional membrane association at low levels during mitosis.

MATERIALS AND METHODS

Fly strains

Tissue-specific expression of UAS-controlled transgenes in NSCs was achieved using a Worniu-GAL4 driver line (Albertson et al., 2004). Lgl dynamics were imaged using Lgl-GFP expressed from its endogenous locus, UAS-Lgl-GFP or UAS-Lgl-mCherry (as noted in figure and movie legends). The endogenous Lgl-GFP line is a MiMIC-based protein trap in which GFP is inserted into the *l(2)gl* locus, resulting in expression of Lgl-GFP under control of the native promoter at endogenous levels. Miranda dynamics were imaged using mira-GFP, a BAC-based genomic rescue construct integrated into a $mira^{KO}$ background (Ramat et al., 2017). Chromosome dynamics were monitored using the marker His2A-RFP. Imaging of aPKC was achieved using a BAC-encoded aPKC-GFP (Besson et al., 2015). Worniu-GAL4 was used to express UAS-RNAi against aPKC and Lgl in NSCs. Knockdown was enhanced through the co-expression of UAS-Dicer2. See Table S1 for details of fly strains.

Live imaging

Third instar larvae were incubated at 29°C for at least 48 h prior to imaging and dissection. Larvae were dissected in Schneider's Insect Media to obtain intact central nervous system explants, which were then mounted on a sterile poly-D-lysine-coated 35 mm glass-bottom dish (ibidi, 81156) containing modified minimal hemolymph-like solution (HL3.1). Larval brain explants were imaged using a Nikon Eclipse Ti-2 Yokogawa CSU-W1 SoRa spinning disk microscope with dual Photometrics Prime BSI sCMOS cameras, utilizing a 60× water immersion objective. GFP-tagged proteins were visualized using 488 nm illumination, while RFP and mCherry tags were visualized using 561 nm illumination. Super-resolution images were captured using super-resolution through optical photon reassignment (SoRa) optics (Azuma and Kei, 2015). NSCs were identified based on size, location within the central nervous system, and expression of Worniu-GAL4-driven transgenes.

To acquire 'dissociated NSCs', *Drosophila* central nervous systems were collected from third instar larvae and incubated for 30 min at 30°C in Schneider's Insect Medium containing 1 mg/ml papain and 1 mg/ml collagenase. After incubation, mechanical dissociation was performed by flushing medium/brains through a pipette tip. The resulting cell suspension was then pelleted using gentle centrifugation (300 ***g*** for 2 min) and washed three times with culture medium consisting of Schneider's Insect Medium containing 10% synthetic fetal bovine serum, 20 mM glutamine, 0.05 mg/ml glutathione and 0.01 mg/ml insulin. After the final wash step, cells were resuspended and plated in culture medium consisting of Schneider's Insect Medium containing 10% synthetic fetal bovine serum, 20 mM glutamine, 0.05 mg/ml glutathione and 0.01 mg/ml insulin and imaged with a Nikon Eclipse Ti-2 Yokogawa CSU-W1 SoRa spinning disk microscope with dual Photometrics Prime BSI sCMOS cameras, using a 60× water immersion objective.

Pharmacological inhibition

The selective Aurora A inhibitor MLN8237 (alisertib; cat. #S1133; Selleckchem; Table S1.) was solubilized in DMSO and used at a working concentration of 15 µM in all relevant experiments.

Image processing and analysis

Imaging data were processed using ImageJ (Fiji package). To correct for photobleaching, the bleach correction tool was used.

Quantification for Fig. 1D,D′

To quantify the dynamics underlying the removal of Lgl from the plasma membrane during early mitosis in NSCs within intact central nervous systems, we used ImageJ to acquire membrane:cytoplasmic ratios for Lgl-GFP signal intensity. To do this, we first measured Lgl membrane intensity by drawing a line of 5-pixel width perpendicular to the membrane traversing from outside the NSC into the cytoplasm at two different locations: the apical pole and lateral membrane. Lgl membrane signal was quantified using the peak signal intensity along the line. Lgl cytoplasmic signal intensity was measured by taking the average signal intensity within a square region of interest drawn inside the NSC cytoplasm, being careful to avoid sampling the nuclear compartment. These measurements allowed us to compare the apical membrane:cytoplasmic ratios to the lateral membrane:cytoplasmic ratios as NSCs moved through early mitosis. The figure depicts the lateral membrane:cytoplasmic ratio at the frame when the apical membrane:cytoplasmic ratio reached ∼1 (i.e. Lgl no longer detectable at the apical pole) for each NSC (n=10).

Quantification for Fig. 1F

To quantify the dynamics of Lgl removal beginning in early prophase in dissociated NSCs, we used ImageJ to acquire membrane:cytoplasmic ratios for Lgl-GFP signal intensity using the method described above for Fig. 1D,D′. This ratio was measured on the apical, lateral and basal sides of each cell (n=3) beginning five frames before the initial apical removal of Lgl, and for five frames following initial apical removal, for a total of 11 frames. The initial apical removal frame was defined as the frame in which the membrane:cytoplasmic of Lgl on the apical side first reached 1. A time course of Lgl removal along the apical, lateral and basal axes was plotted using GraphPad Prism 10. The figure depicts time 0 as initial apical Lgl removal. These measurements allowed us to compare the apical, lateral and basal membrane:cytoplasmic ratios before, during and following Lgl removal.

Quantification for Fig. 1H

To quantify the dynamics of Lgl membrane recruitment at mitotic exit in dissociated NSCs, we used the same method of obtaining membrane: cytoplasmic ratios for Lgl-GFP on the apical, lateral and basal sides of each cell (n=3) as described for Fig. 1F. We measured these ratios beginning five frames prior to the initial recruitment of Lgl to the intracellular bridge (ICB), and for five frames after initial recruitment to the ICB for a total of 11 frames. We defined initial ICB recruitment as the first frame in which Lgl signal was detectable at the ICB. A time course of Lgl recruitment along the ICB, lateral and apical axes was plotted using GraphPad Prism 10. The figure depicts time 0 as the first frame containing a detectable Lgl signal at the ICB.

Quantification for Fig. 2B

To quantify the effects of aPKC knockdown on Lgl membrane binding over the course of the cell cycle, apical membrane:cytoplasmic ratios for Lgl-GFP signal intensity were measured (as described for Fig. 1D). Ratios were measured at three different time points in the cell cycle. In all the NSCs we sampled, NSCs were in the process of rounding up at 7 min prior to nuclear envelope breakdown (NEB), and we therefore used this as the 'prophase' time point. We used the frame before anaphase onset as the 'metaphase' time point. NSCs expressing aPKC-RNAi were compared to control cells not expressing RNAi (wild type).

Quantification for Fig. 2D

To quantify the effects of Aurora A inhibition on the removal of Lgl from the plasma membrane during early mitosis, apical membrane:cytoplasmic ratios for Lgl-GFP signal intensity were measured (as described for Fig. 1D). 'Prophase' measurements were taken at 6 min and 40 s prior to NEB. 'Metaphase' measurement were taken at 20 s prior to anaphase onset. NSCs treated with the Aurora A inhibitor solubilized in DMSO were compared to control cells treated with DMSO alone.

Quantification for Fig. 3B

To determine whether the removal of Lgl from the apical membrane is spatially and temporally correlated with the recruitment of aPKC to the apical membrane during mitotic entry, we used NSCs expressing Lgl-mCherry and aPKC-GFP (n=6) to measure the apical membrane: cytoplasmic ratio for both aPKC and Lgl over the course of Lgl removal/ aPKC recruitment. Time 0 was defined as the frame in which apical Lgl first reached the limit of detection (membrane:cytoplasmic ratio of ∼1). Fig. 3B depicts the apical membrane:cytoplasmic ratio of Lgl-mCherry signal intensity and the apical membrane:cytoplasmic ratio of aPKC-GFP signal intensity 5 min prior to Lgl removal, at initial Lgl removal, and 5 min following Lgl removal.

Quantification for Fig. 3D

To determine whether the removal of aPKC from the membrane is spatially and temporally correlated with the recruitment of Lgl to the membrane, we performed dual imaging of NSCs expressing Lgl-mCherry and aPKC-GFP (n=7). The quantification depicts measurements taken during mitotic exit, with time 0 being at the frame in which aPKC-GFP signal near the ICB reached the limit of detection (membrane:cytoplasmic ratio of ∼1). Measurements were also taken 5 min prior to this time point, and 5 min afterwards.

Quantification for Fig. 4B

To quantify the effects of Lgl knockdown on aPKC localization at the apical membrane, apical membrane:cytoplasmic ratios for aPKC-GFP signal intensity were measured at interphase (15 min prior to NEB), prophase (7 min prior to NEB) and metaphase (1 min before anaphase onset). NSCs expressing Lgl-RNAi (n=5) were compared to wild-type NSCs (n=5).

Quantification for Fig. 4C

To quantify the effects of Lgl knockdown on aPKC localization at the basal membrane, basal membrane:cytoplasmic ratios for aPKC-GFP signal intensity were measured at metaphase (1 min before anaphase onset). NSCs expressing Lgl-RNAi (n=5) were compared to wild-type NSCs (n=5).

Quantification for Fig. 4D

To quantify the effects of Lgl knockdown on aPKC polarity, the apical aPKC membrane:cytoplasmic ratio in Lgl-RNAi cells (n=6) was measured at two time points: during prophase, which was defined as 7 min before nuclear envelope breakdown, and later at metaphase (one frame before anaphase onset).

Quantification for Fig. 4F

To quantify the effects of Lgl knockdown on the ability of Miranda to localize to the basal membrane during metaphase, we measured the basal Miranda membrane:cytoplasmic ratio at metaphase in both Lgl-RNAi cells (n=7) and wild-type cells (n=7). Metaphase was defined as the frame before anaphase onset.

Quantification for Fig. 4H

To quantify the effects of Lgl knockdown on Miranda localization during interphase, we measured the apical membrane:cytoplasmic ratio of Miranda signal intensity in both wild-type and Lgl-RNAi NSCs (n=7). Interphase was defined as 18 min and 40 s before anaphase onset, a time point when all cells had not yet begun to round up.

Statistical analysis

Gardner–Altman estimation plots and 95% confidence intervals of datasets were prepared using the DABEST package (Ho et al., 2019). Statistical details can be found in the relevant figure legends.

Acknowledgements

We thank Eurico Morais-de-Sá for helpful discussions, Sarah Siegrist for a detailed dissociated NSC protocol, and Adam Fries for maintaining the microscope used in this study.

Competing interests

The authors declare no competing or financial interests.

Author contributions

Conceptualization: S.E.W., B.L., K.E.P.; Data curation: S.E.W., B.L.; Formal analysis: S.E.W., B.L., K.E.P.; Funding acquisition: B.L., K.E.P.; Investigation: S.E.W., B.L.; Methodology: K.E.P.; Project administration: K.E.P.; Supervision: B.L., K.E.P.; Writing – original draft: S.E.W., B.L., K.E.P.; Writing – review & editing: S.E.W., B.L., K.E.P.

Funding

This work was supported by National Institute of General Medical Sciences grants (R35GM127092 and K99GM147601 to K.E.P. and B.L., respectively).

Data and resource availability

All relevant data and details of resources can be found within the article and its supplementary information.

Peer review history

The peer review history is available online at https://journals.biologists.com/jcs/lookup/doi/10.1242/jcs.264687.reviewer-comments.pdf

References

Albertson, R., Chabu, C., Sheehan, A. and Doe, C. Q. (2004). Scribble protein domain mapping reveals a multistep localization mechanism and domains necessary for establishing cortical polarity. *J. Cell Sci.* **117**, 6061-6070. doi:10.1242/jcs.01525

Atwood, S. X., Chabu, C., Penkert, R. R., Doe, C. Q. and Prehoda, K. E. (2007). Cdc42 acts downstream of Bazooka to regulate neuroblast polarity through Par-6 aPKC. *J. Cell Sci.* **120**, 3200-3206. doi:10.1242/jcs.014902

Azuma, T. and Kei, T. (2015). Super-resolution spinning-disk confocal microscopy using optical photon reassignment. *Opt. Express.* **23**, 15003-15011. doi:10.1364/OE.23.015003

Bailey, M. J. and Prehoda, K. E. (2015). Establishment of par-polarized cortical domains via phosphoregulated membrane motifs. *Dev. Cell.* **35**, 199-210. doi:10.1016/j.devcel.2015.09.016

Bell, G. P., Fletcher, G. C., Brain, R. and Thompson, B. J. (2015). Aurora kinases phosphorylate Lgl to induce mitotic spindle orientation in Drosophila epithelia. *Curr. Biol.* **25**, 61-68. doi:10.1016/j.cub.2014.10.052

Besson, C., Bernard, F., Corson, F., Rouault, H., Reynaud, E., Keder, A., Mazouni, K. and Schweisguth, F. (2015). Planar cell polarity breaks the symmetry of PAR protein distribution prior to mitosis in Drosophila sensory organ precursor cells. *Curr. Biol.* **25**, 1104-1110. doi:10.1016/j.cub.2015.02.073

Betschinger, J., Mechtler, K. and Knoblich, J. A. (2003). The Par complex directs asymmetric cell division by phosphorylating the cytoskeletal protein Lgl. *Nature* **422**, 326-330. doi:10.1038/nature01486

Betschinger, J., Mechtler, K. and Knoblich, J. A. (2006). Asymmetric segregation of the tumor suppressor brat regulates self-renewal in Drosophila neural stem cells. *Cell* **124**, 1241-1253. doi:10.1016/j.cell.2006.01.038

Buckley, C. E. and St Johnston, D. (2022). Apical-basal polarity and the control of epithelial form and function. *Nat. Rev. Mol. Cell Biol.* **23**, 559-577. doi:10.1038/s41580-022-00465-y

Carvalho, C. A., Moreira, S., Ventura, G., Sunkel, C. E. and Morais-de-Sá, E. (2015). Aurora A triggers Lgl cortical release during symmetric division to control planar spindle orientation. *Curr. Biol.* **25**, 53-60. doi:10.1016/j.cub.2014.10.053

Dong, W., Zhang, X., Liu, W., Chen, Y.-J., Huang, J., Austin, E., Celotto, A. M., Jiang, W. Z., Palladino, M. J., Jiang, Y. et al. (2015). A conserved polybasic domain mediates plasma membrane targeting of Lgl and its regulation by hypoxia. *J. Cell Biol.* **211**, 273-286. doi:10.1083/jcb.201503067

Grifoni, D., Garoia, F., Bellosta, P., Parisi, F., De Biase, D., Collina, G., Strand, D., Cavicchi, S. and Pession, A. (2007). aPKCzeta cortical loading is associated with Lgl cytoplasmic release and tumor growth in Drosophila and human epithelia. *Oncogene* **26**, 5960-5965. doi:10.1038/sj.onc.1210389

Ho, J., Tumkaya, T., Aryal, S., Choi, H. and Claridge-Chang, A. (2019). Moving beyond P values: data analysis with estimation graphics. *Nat. Methods* **16**, 565-566. doi:10.1038/s41592-019-0470-3

Holly, R. W., Jones, K. and Prehoda, K. E. (2020). A Conserved PDZ-Binding Motif in aPKC Interacts with Par-3 and Mediates Cortical Polarity. *Curr. Biol.* **30**, 893-898.e5. doi:10.1016/j.cub.2019.12.055

Hutterer, A., Betschinger, J., Petronczki, M. and Knoblich, J. A. (2004). Sequential roles of Cdc42, Par-6, aPKC, and Lgl in the establishment of epithelial polarity during Drosophila embryogenesis. *Dev. Cell* **6**, 845-854. doi:10.1016/j.devcel.2004.05.003

Ikeshima-Kataoka, H., Skeath, J. B., Nabeshima, Y., Doe, C. Q. and Matsuzaki, F. (1997). Miranda directs Prospero to a daughter cell during Drosophila asymmetric divisions. *Nature* **390**, 625-629. doi:10.1038/37641

Lang, C. F. and Munro, E. (2017). The PAR proteins: from molecular circuits to dynamic self-stabilizing cell polarity. *Development* **144**, 3405-3416. doi:10.1242/dev.139063

Lee, C.-Y., Andersen, R. O., Cabernard, C., Manning, L., Tran, K. D., Lanskey, M. J., Bashirullah, A. and Doe, C. Q. (2006a). Drosophila Aurora-A kinase inhibits neuroblast self-renewal by regulating aPKC/Numb cortical polarity and spindle orientation. *Genes Dev.* **20**, 3464-3474. doi:10.1101/gad.1489406

Lee, C.-Y., Robinson, K. J. and Doe, C. Q. (2006b). Lgl, Pins and aPKC regulate neuroblast self-renewal versus differentiation. *Nature* **439**, 594-598. doi:10.1038/nature04299

Lee, C.-Y., Wilkinson, B. D., Siegrist, S. E., Wharton, R. P. and Doe, C. Q. (2006c). Brat is a Miranda cargo protein that promotes neuronal differentiation and inhibits neuroblast self-renewal. *Dev. Cell.* **10**, 441-449. doi:10.1016/j.devcel.2006.01.017

Matsuzaki, F., Ohshiro, T., Ikeshima-Kataoka, H. and Izumi, H. (1998). miranda localizes staufen and prospero asymmetrically in mitotic neuroblasts and epithelial cells in early Drosophila embryogenesis. *Development* **125**, 4089-4098. doi:10.1242/dev.125.20.4089

Moreira, S. and Morais-de-Sá, E. (2016). Spatiotemporal phosphoregulation of Lgl: finding meaning in multiple on/off buttons. *Bioarchitecture* **6**, 29-38. doi:10.1080/19490992.2016.1149290

Moreira, S., Osswald, M., Ventura, G., Gonçalves, M., Sunkel, C. E. and Morais-de-Sá, E. (2019). PP1-mediated dephosphorylation of Lgl controls apical-basal polarity. *Cell Rep.* **26**, 293-301.e7. doi:10.1016/j.celrep.2018.12.060

Ohshiro, T., Yagami, T., Zhang, C. and Matsuzaki, F. (2000). Role of cortical tumour-suppressor proteins in asymmetric division of Drosophila neuroblast. *Nature* **408**, 593-596. doi:10.1038/35046087

Oon, C. H. and Prehoda, K. E. (2019). Asymmetric recruitment and actin-dependent cortical flows drive the neuroblast polarity cycle. *eLife* **8**, e45815. doi:10.7554/eLife.45815

Oon, C. H. and Prehoda, K. E. (2021). Phases of cortical actomyosin dynamics coupled to the neuroblast polarity cycle. *eLife* **10**, e66574. doi:10.7554/eLife.66574

Peng, C. Y., Manning, L., Albertson, R. and Doe, C. Q. (2000). The tumour-suppressor genes lgl and dlg regulate basal protein targeting in Drosophila neuroblasts. *Nature* **408**, 596-600. doi:10.1038/35046094

Ramat, A., Hannaford, M. and Januschke, J. (2017). Maintenance of miranda localization in Drosophila neuroblasts involves interaction with the cognate mRNA. *Curr. Biol.* **27**, 2101-2111.e5. doi:10.1016/j.cub.2017.06.016

Rolls, M. M., Albertson, R., Shih, H.-P., Lee, C.-Y. and Doe, C. Q. (2003). Drosophila aPKC regulates cell polarity and cell proliferation in neuroblasts and epithelia. *J. Cell Biol.* **163**, 1089-1098. doi:10.1083/jcb.200306079

Schuldt, A. J., Adams, J. H. J., Davidson, C. M., Micklem, D. R., Haseloff, J., Johnston, D. S. and Brand, A. H. (1998). Miranda mediates asymmetric protein and RNA localization in the developing nervous system. *Genes Dev.* **12**, 1847-1857. doi:10.1101/gad.12.12.1847

Shen, C.-P., Jan, L. Y. and Jan, Y. N. (1997). Miranda is required for the asymmetric localization of prospero during mitosis in Drosophila. *Cell* **90**, 449-458. doi:10.1016/S0092-8674(00)80505-X

Sunchu, B. and Cabernard, C. (2020). Principles and mechanisms of asymmetric cell division. *Development* **147**, dev167650. doi:10.1242/dev.167650

Venkei, Z. G. and Yamashita, Y. M. (2018). Emerging mechanisms of asymmetric stem cell division. *J. Cell Biol.* **217**, 3785-3795. doi:10.1083/jcb.201807037

Wirtz-Peitz, F., Nishimura, T. and Knoblich, J. A. (2008). Linking cell cycle to asymmetric division: aurora-A phosphorylates the Par complex to regulate Numb localization. *Cell* **135**, 161-173. doi:10.1016/j.cell.2008.07.049

Yamanaka, T., Horikoshi, Y., Izumi, N., Suzuki, A., Mizuno, K. and Ohno, S. (2006). Lgl mediates apical domain disassembly by suppressing the PAR-3-aPKC-PAR-6 complex to orient apical membrane polarity. *J. Cell Sci.* **119**, 2107-2118. doi:10.1242/jcs.02938